2021-08

Feedforward control algorithms for MEMS galvos and scanners

Feedforward Control Algorithms for MEMS Galvos and Scanners

Lawrence K. Barrett, Matthias Imboden, Joshua Javor, David K. Campbell, and David J. Bishop, *Member, IEEE*

***Abstract*— Optical systems typically use galvanometers (galvos) and scanners. Galvos move, quasi-statically, from one static position to another. Scanners move in an oscillatory fashion, typically at the device resonant frequency. MEMS devices, which have many advantages and are often used in optical systems, are typically high Q devices. Moving from one position to another for a galvo or one amplitude to another for scanners, can take many periods to settle following the ring down. During these transitions, the optical system is inactive. Here, we show how precisely timed pulses can be used (in an open loop manner) to begin or end scanner motion without ring up/ring down time. The size of pulse required is found to depend on the Q of the device, and relationships are derived. The pulse can also be separated into multiple pulse spaced one period apart if pulses of the necessary size are not possible due to constraints of the physical device. For finite Q scanners, the amplitude decreases after the initial pulse due to damping. This can be eliminated by applying an excitation at the frequency of the scanner. The necessary amplitude for this excitation is derived. Finally, by combining this open loop control algorithm with an open loop control algorithm for galvo motion the device can seamlessly move between scanner and galvo functioning. These control algorithms are demonstrated using computer simulations, analytical models and a commercially available MEMS mirror (Mirrorcle Technologies, A8L2.2). [2020-0238]**

***Index Terms*— MEMS, galvanometers, galvos, scanners, step and settle time, open loop controls.**

Manuscript received June 12, 2020; revised December 19, 2020; accepted February 18, 2021. This work was supported in part by the National Science Foundation under Grant EEC-1647837, Grant ECCS-1708283, and Grant EEC-0812056; in part by the SONY Faculty Innovation Award; and in part by the Defense Advanced Research Projects Agency/Air Force Research Lab (DARPA/AFRL) under Award FA8650-15-C-7545. Subject Editor C. Rembe. *(Corresponding author: Lawrence K. Barrett.)*

Lawrence K. Barrett is with the Division of Materials Science and Engineering, Boston University, Boston, MA 02215 USA (e-mail: blawrenc@bu.edu).

Matthias Imboden is with 4K-MEMS, 2072 Saint-Blaise, Switzerland (e-mail: m.imboden@4kmems.ch).

Joshua Javor is with the Department of Mechanical Engineering, Boston University, Boston, MA 02215 USA (e-mail: jjavor@bu.edu).

David K. Campbell is with the Department of Physics, Boston University, Boston, MA 02215 USA, also with the Division of Materials Science and Engineering, Boston University, Boston, MA 02215 USA, and also with the Department of Electrical and Computer Engineering, Boston University, Boston, MA 02215 USA (e-mail: dkcampbe@bu.edu).

David J. Bishop is with the Division of Material Science and Engineering, Boston University, Boston, MA 02215 USA, also with the Department of Electrical and Computer Engineering, Boston University, Boston, MA 02215 USA, also with the Department of Physics, Boston University, Boston, MA 02215 USA, also with the Department of Mechanical Engineering, Boston University, Boston, MA 02215 USA, and also with the Department of Biomedical Engineering, Boston University, Boston, MA 02215 USA (e-mail: djb1@bu.edu).

This article has supplementary material provided by the authors and color versions of one or more figures available at https://doi.org/10.1109/JMEMS.2021.3074301.

Digital Object Identifier 10.1109/JMEMS.2021.3074301

I. Introduction

MEMS devices are playing a large and growing role in transducing the electronic domain into the mechanical [1]–[3]. In the world of MEMS actuators, devices that turn electrical controls into motion, modes of operation tend to fall into two broad classes. There is quasi-static operation where the device is moved from one static position to another and the figure of merit is the step and settle response time [4]–[9]. In optical systems, these types of devices are called galvanometers or "galvos".[1] The other typical mode of operation is scanning where the MEMS device continuously oscillates, usually at its resonant frequency, to leverage the Q of the system [10], [11]. In optics, these types of devices are called "scanners" and can run along one or two axes. Here we discuss how they both can be operated with open loop control algorithms and achieve essentially ideal behavior.

These two types of operation, quasi-static and scanning, are widely used because they represent two stable states for a moderately high Q MEMS device, oscillating at resonance or being static [12], [13]. The optical engineer can design the system to do something useful, such as imaging in a LIDAR system, while the device is doing one of these [14], [15]. Using normal drive methods, transitioning from one of these states to the other requires waiting a multitude of periods of the device for the ringing behavior to end, and this temporal overhead limits system performance.

In this article, we show how a novel open loop control theory algorithm allow the turning on and off of specific modes of scanner with transitions between them that take only a fraction of a period. Furthermore, we show how they can be combined with an open loop control algorithm for galvos described previously by Imboden *et al.* which allows galvos to transition in less than a period as well [16]. Combining these algorithms allows MEMS devices to move seamlessly between scanner and galvo functioning creating complex responses. These algorithms are demonstrated here with computer simulations, analytical models, and experimentally.

II. Background

Figure 1 shows an example of what we discuss here. In the upper panel is shown the ability to turn the fundamental mode of the device on and off, precisely and quickly. This is a

[1]First galvanometers were used as current sensors, the name has been appropriated by systems where a mirror is moved by applying a current in order to position light. The sensor became an actuator.

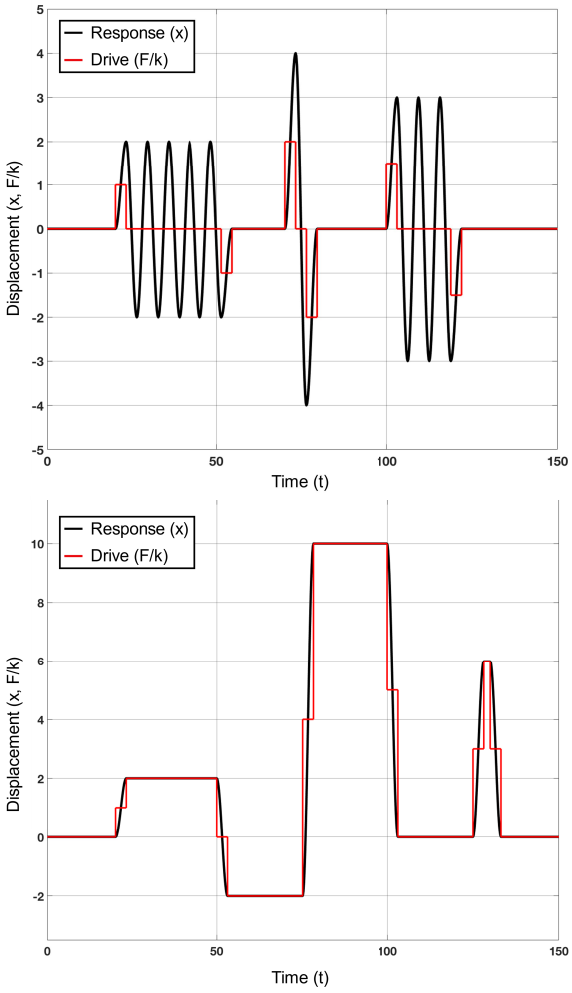

Fig. 1. Shown in the upper panel is the open loop algorithm for scanner motion. The algorithm allows the modes of the system to be turned on and off, with precision. The lower panel shows the open loop algorithm for galvos. Both results are for the same infinite Q system. The red curve is the applied drive (F/k, see equation 1) and the black curve, the system response (x, see equation 1). This is a Simulink simulation.

Simulink simulation for an infinite Q system with a 1 rad/s resonant frequency. It would normally take an infinite time to make these transitions. As one can see, it is possible to abruptly turn these modes on and off, in integral units of the half period of the device. This is the behavior of an optimal scanner device. The lower panel shows how this same system can be made to operate quasi-statically, moving from one static position to another, quickly, with each transition taking one half of a period. Once again, this is for an infinite Q system. This is the behavior of an optimal galvo device. Combining these two methods lets one move the device to any position, to oscillate a specific number of cycles and then return to some other position. We have demonstrated this performance in Figure 1 for an infinite Q system but our approaches are perfectly general and will work for any underdamped, second order system with a $Q > 1$.

A previous set of papers [6], [16]–[18] have discussed the galvo behavior of a MEMS device and shown how it can have essentially perfect step and settle behavior. We will briefly summarize those results here. For a high Q system, when you apply a step function input, the system overshoots to twice the final rest position and then oscillates about that final rest position until it finally converges to that point. If, instead, a half-step is applied, one half a period later, the system is at a peak of its excursion with an amplitude equal to the desired final rest position. With zero slope in a position-time plot, its velocity is zero. The method shown in the lower panel of Figure 1 applies half the value of the force needed to hold the device at its desired end position and after one half a period, applies the full force. With the device where it is intended to be, after half a period, with zero velocity, this application of the full force essentially catches it and holds it in the desired position, stably for as long is desired. This is called a double step (DS) drive. One half the force and one half the period are the values for an infinite Q ($Q > 100$) system. This is perfectly general and works for a system with any Q with a modification of the parameters. This is derived later in the analytical section. Ref. 17 discusses a variety of similar drive schemes called overdrive methods where one applies an accelerating force for a while and then a decelerating force. They are similar to how one moves an object in free space where it starts at rest, an accelerating force is applied, and then a decelerating force is applied with the object arriving at its final rest position with zero velocity. The simulation shown in the lower panel of Figure 1 was obtained using DS for all the transitions. The drive signal is the red curve and one can see the double step structure for each transition. These open loop drive schemes allow for essentially ideal galvo behavior. If a system does not allow design of the open loop drive, one may alter the micromechanical design to optimize step-and-settle behavior. However, this method requires design tradeoffs and the improvement in settling time is limited, as was shown by a 5-fold improvement using a MEMS mirror previously [19].

In this paper, our main focus is the behavior shown in the upper panel of Fig. 1. This is the control algorithm for scanner functioning. The key to our approach is to drive the system coherently, with full knowledge of its underlying dynamics. In a conventional control theory approach [12], [13], one uses feedback and methods like PID control. Our approach here is simpler from a system point of view because the sensor and feedback system are not needed, reducing cost and complexity. The high stability and linearity of MEMS make them ideally suited for such feedforward control algorithms [20].

This paper is organized into the following sections. In section IIA we present results from Simulink simulations using an infinite Q system, demonstrating all tools we have at our disposal. In section IIB we study a finite Q system showing how finite damping modifies the algorithms demonstrated in section IIA. In section III, we present a closed-form solution of the underlying equations of motion for our system. Finally, in section IV, we present experimental results on a MEMS micromirror. This analysis and data are for a MEMS application, but we note that these approaches will work equally well for any underdamped, second order system.

A. Infinite Q Systems

In this section we discuss results obtained using Simulink simulations on an infinite Q, second order system. The

system has a resonant frequency of 1 rad/s, the period is 2π. The simulations are performed with time steps of 10^{-4} seconds and typically cover periods of time in the range of 100-300 seconds. If one gives the system a step input, one sees the behavior shown in Figure 2a). It rings forever, oscillating between zero and twice the nominal final resting place. A larger step increases the oscillating amplitude. If one turns the step off at an arbitrary time, the device ends up in a non-determinate state. The signal shown in Figure 2a) is unipolar, it oscillates between zero and twice the nominal resting point of the system. If one wishes to have bipolar behavior, one can use a pulse like that shown in Figure 2b). One half a period (π) after the step up, a step down in equal amplitude is applied. In this case the system oscillates symmetrically around zero.

In figure 2(c), the step duration lasts precisely four device periods (8π). One can see that the modes have been completely and cleanly turned off. The key point is to apply the off transition at a very specific time in the oscillation cycle to pull the energy out of the mode. In this example, after four periods (or any integer number) the kinetic energy is zero. By switching the offset to zero all potential energy is removed from the mode as well and hence, the resonator remains at rest. We note that by applying this method, even a dissipation free system, which would normally result in an infinite settling time can be made to switch on and off in a single period (half period for each transition). We also note these are open loop drive algorithms, there is no feedback being employed. The amplitude of oscillation is determined by the pulse amplitude.

Shown in Figure 1 upper panel, one can also use a negative pulse applied at an integer number of periods after the first pulse (in this case 5 periods or 10π) to turn a bipolar the sequence off. One can have as few as one complete cycle or even a half a cycle. For the single full cycle, 1.5 periods long, one applies a step up, half a period later one has the step down to zero, half a period later a step down to minus the step-up amplitude and finally, a half a period later a step up to zero. To obtain the unipolar signal one applies a pulse of a full period length. When the system is at rest, a step up can be applied at any time. The key to the approach we present here is to apply the rest of the pulse sequence at times that correspond to integer values of the device period, which for MEMS devices may be known to 1 ppm or better. We are using an understanding of the device dynamics to time our pulses to let us turn these modes on and off at will.

For a linear system, one can combine the techniques shown in the upper (scanner functioning) and lower (galvo functioning) panels of Figure 1 to produce complex patterns. An example of such a pattern is shown in Figure 3. In this figure, we use the DS drive (start and stop) to create a plateau and then use the recipe for a full sine wave to put a negative pulse in the center of the plateau. With the tools presented here one can create an essentially unlimited set of patterns and behaviors of arbitrary complexity. Each transition lasts half a period, with, unless desired, no overshoot or ringing. One can engineer the modes of the MEMS device to meet the needs of the imaging system as opposed to designing the optics around the limitations of the MEMS device.

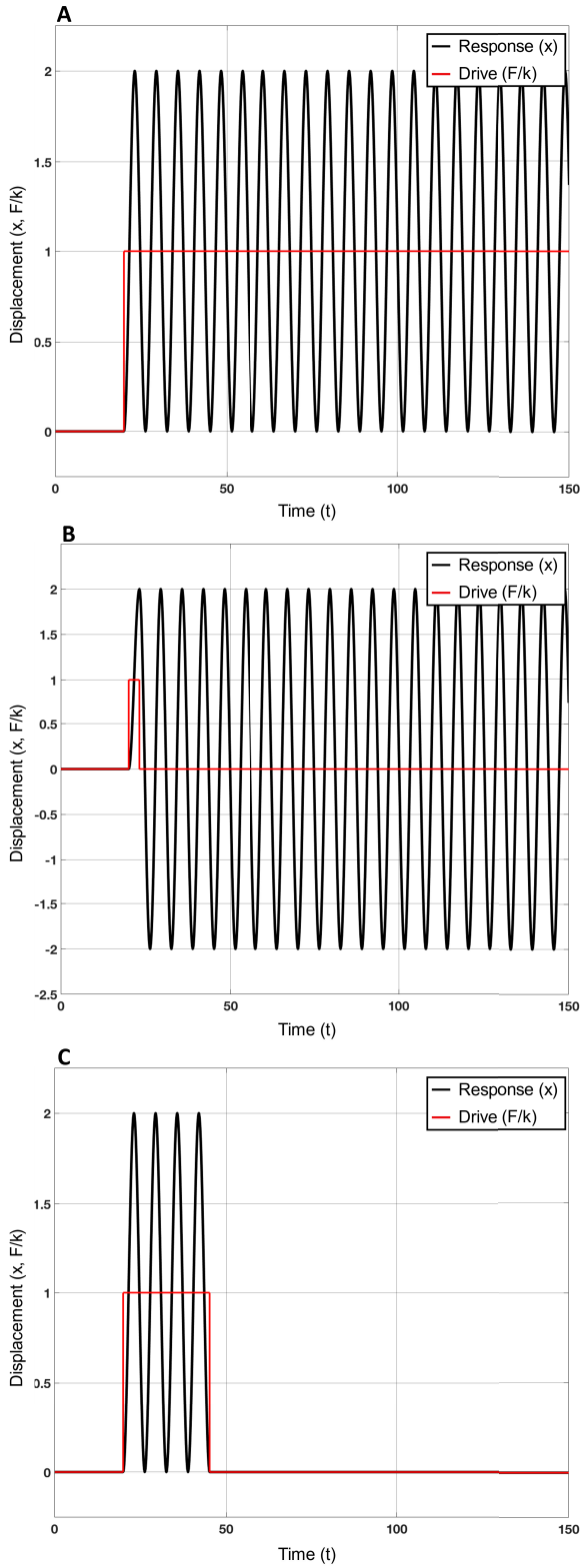

Fig. 2. Shown are Simulink simulations on an infinite Q system. (a) a response to a step. The system oscillates in a unipolar way, between zero and twice the equilibrium position. (b) when a half period pulse is applied, the system rings in a bipolar way. (c) a properly timed step down turns the oscillations off.

In this section, we have discussed applying the scanner control algorithm to an infinite Q system. However, the techniques are general and can be applied to finite Q systems. In the next section, we discuss these methods.

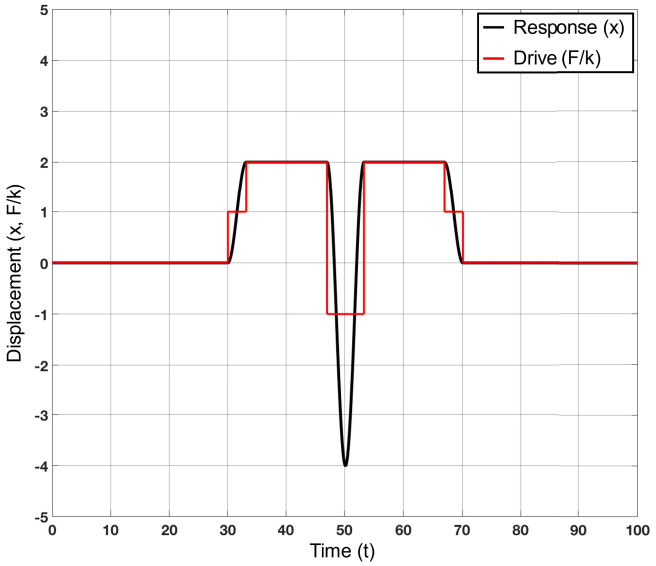

Fig. 3. Shown is an example of using galvo control (Fig. 1) and scanner control algorithms (Fig. 3) to produce a complex response. This is a Simulink simulation for an infinite Q system. The red trace is the applied drive and the black curve is the system response.

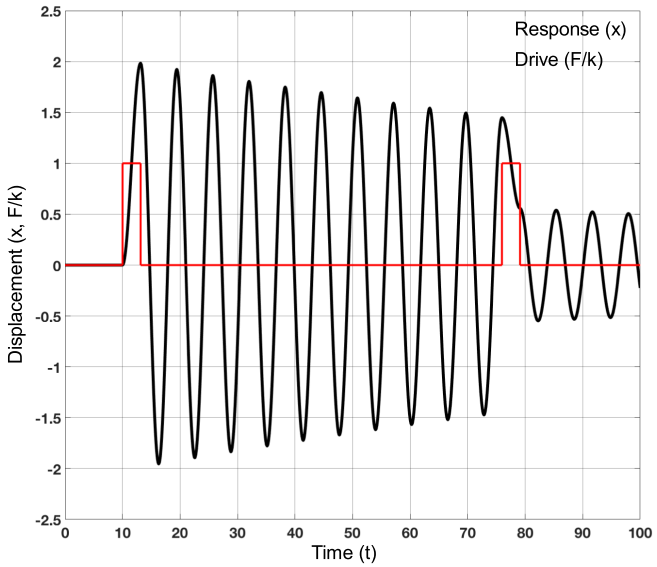

Fig. 4. Shown is an 11 pulse cycle for an infinite Q system, upper panel and a system with a Q of 100, lower panel. These are Simulink simulations with the red traces the input and the black curves the system response.

B. Finite Q Systems

For a system with a finite Q, one needs to modify the algorithms discussed previously. Finite Q causes two effects, one related to timing, and the other effects is that the dissipation must be compensated to ensure the desired amplitude is reached. The timing effect is the shift in resonant frequency due to finite damping. One needs to use the true resonant frequency of the system for the timing as discussed above, which takes the dissipation into account. To compensate the loss in the amplitude response the forcing must be adjusted accordingly

Finite Q means losses in energy and hence amplitude of the oscillating mode. Figure 4 shows what happens. In the upper panel of Figure 4, the system has an infinite Q and behaves as described previously. In the lower panel, the system has a Q of $\sim$100 and two things happen. Because energy is lost every cycle, the amplitude of the oscillating mode decays over time. And because the amplitude of the final cycle is not the amplitude of the first cycle, the second pulse stops the oscillator before it reaches the zero point. When the second pulse is completed the oscillator is not at the origin or at rest. Now when the pulse is switched off the mode continues to ring with a non-zero amplitude. The energy lost during the ring-down must be compensated to maintain the desired amplitude. To do this we add in a small amount of drive at the resonant frequency.

Figure 5 shows how this is done. Enough energy is added at the resonant frequency to compensate for the damping losses by adding a unipolar square wave. We are, in essence, topping up the mode. This returns the response of the system to the ideal behavior seen for the infinite Q performance. The other transition pulses demonstrated for the infinite Q system can also be modified in a similar way.

In the infinite Q limit, the emptying pulse is equal in amplitude to the initial pulse, and no energy is dissipated

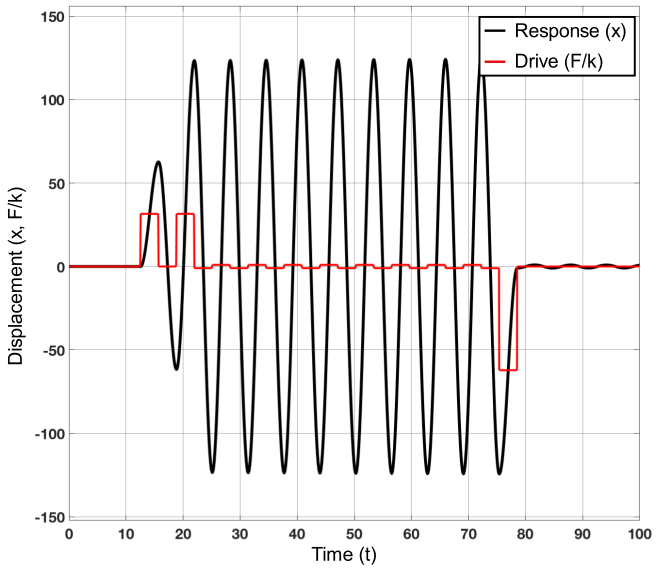

Fig. 5. Shown is a Simulink simulation of a system with a Q $\sim$ 100. Three new features are demonstrated: 1. one can ring the system up (or down) in multiple pulses, 2. we are using a square wave to keep the mode topped up and 3. we can use a negative pulse, moved by 1/2 a period, to remove the energy from the mode. The red curve is the input and the black the response.

during the ringing of the system. For finite Q, the starting pulse is larger than the stopping pulse. This is because the starting pulse needs to add in some extra energy to account for the losses during the first cycle and the last pulse needs less energy because of losses during the last cycle. This equivalence is shown explicitly in the analytical section.

Figure 4 and 5 demonstrate that by shifting the emptying pulse by one half a period, one can use either a positive going pulse instead or a negative going pulse to bring the resonator to rest. This feature allows one to tailor the drive to match the electronics and forcing amplitudes one has available.

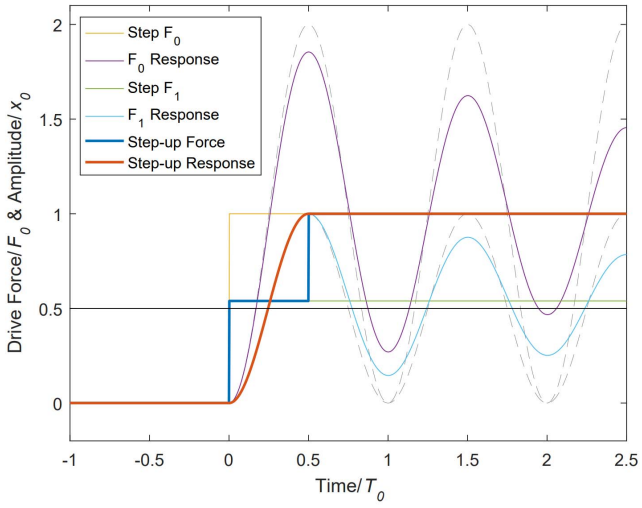

Fig. 6. Shown is the single step and two-step response for a Q = 10 system (infinite Q response is dashed), calculated using the closed form solution 4 and 5. The red trace depicts the set and hold response, illustrating a transition with no ringing or overshoot.

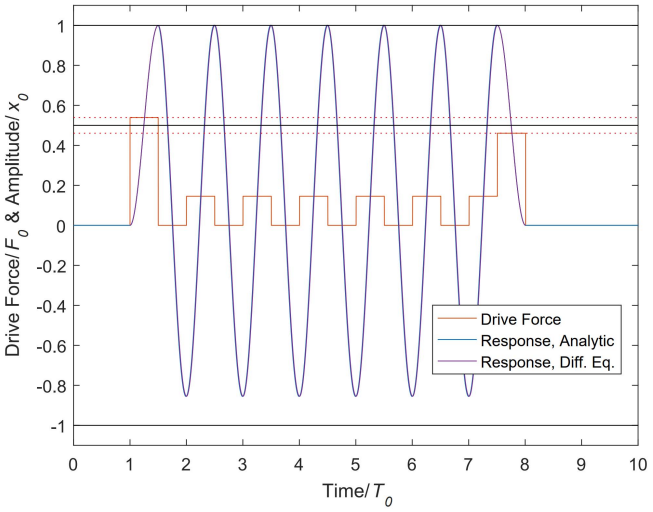

Fig. 7. Shown is the response for a system with a Q of 10 with the applied pulse train in red (square wave unipolar drive). The analytic solution reproduces perfectly the numeric solution to the differential equation. The lower black line illustrates the amplitude of the first and last pulse for a dissipation free system, the dashed lines illustrate the drive forces needed to add and remove the energy from the mode. The upper black line represents the displacement amplitude for a dissipation free system.

Figure 5 also shows that one can fill the mode initially (or empty it) using multiple timed pulses one period apart (this is a quasi-ring-up approach). The amplitude of the excitation is the same for a single pulse and multiple smaller pulses if the sum of the amplitudes of the smaller pulses equal the amplitude of the single pulse. This may work better experimentally where the ability to apply large forces may be limited.

It should be added that if the systems are not driven harmonically on resonance even high Q systems will have a limited amplitude response. This is compensated by higher drive forces. While the maximum applied force may be limited, for example by the maximum voltage or current available, the technique described is also limited in the response amplitude by the requirement that the resonator remains in the linear regime. The derivations in the Analytical Results Section assume that the resonators behave as linear springs. It is furthermore assumed that the forcing can be linearized (for example, for a comb capacitor the amplitude scales as the square of the applied voltage, the force is thus treated as linear with respect to V^2).

III. Analytical Models

In this section, we discuss the analytical solution to the relevant ordinary differential equations (ODEs). As shown above, one can drive the system using pulses comprising parts of square waves or parts of sine waves. For the sake of simplicity, we discuss the use of square wave pulses in this section. To maximize the functionality of a potential device, it is desirable to combine the drive scheme for scanners (Figure 6) with the drive scheme for galvos (Figure 7). Both, these drive schemes can be created by various combinations of step functions with appropriate time delays and changes in step height. Because our system is linear, we can create the complete analytical result of these combine drive schemes by summing the contributions to create our final system response. In this section, for simplicity, we focus on a system with finite $Q = \frac{m\omega_0}{\gamma}$ whose natural frequency is $\omega_0 = \sqrt{\frac{k}{m}}$, mass m and loss factor γ. The resonator is further characterized by its spring constant k and can be driven by static forces F_1 and squarewave forcing F_{dr} at a frequency of ω_{dr}. The resonance frequency includes dissipative effects and is expressed as $\omega_r = \omega_0\sqrt{1-\left(\frac{\gamma}{2m\omega_0}\right)^2} = \frac{2\pi}{T_r}$, and T_r is the period of the resonance. Such a system is characterized by the following second order differential equation:

$$m\ddot{x} + \gamma\dot{x} + kx = F_1 + F_{dr}(t), \tag{1}$$

where $F_{dr}(t)$, represents square wave forcing and is defined:

$$F_{dr}(t) = \operatorname{sgn}(\sin\omega_{dr}t)$$

The response takes the general form

$$\begin{aligned} x(t) = {} & \frac{F_1}{k} + e^{-\frac{\gamma}{2m}t}e^{-it\omega_0\sqrt{1-\left(\frac{\gamma}{2m\omega_0}\right)^2}} \\ & \times \left(a + e^{-2it\omega_0\sqrt{1-\left(\frac{\gamma}{2m\omega_0}\right)^2}}b\right) \\ & + F_{dr}\frac{m\left(\omega_0^2-\omega_{dr}^2\right)\sin(\omega_{dr}t) - \gamma\omega_{dr}\cos(\omega_{dr}t)}{(\gamma\omega_{dr})^2 + m^2\left(\omega_0^2-\omega_{dr}^2\right)^2}, \end{aligned} \tag{2}$$

All the simulations outlined above can be expressed by applying the driving conditions and the boundary conditions and solving for the integration constants a and b. Without loss of generality we define the target amplitude to be x_0, which is reached by the static force $F_0 = kx_0$.

For example, the ring free step-up depicted in Figure 6 is obtained by setting $F_{dr} = 0$, $x(0) = 0$ and $x'(0) = 0$. The last free parameter is F_1, is determined by requiring that the

apex is reached after the first half period, or $x(t_1) = x_0$, note that $t_1 = \frac{1}{2}T_r$. The solution is the well-known expression for the response of a harmonic oscillator to the step drive:

$$x(t) = \frac{F_1}{k}\left(1 - e^{-\frac{\gamma t}{2m}}\left(\cos(\omega_r t) + \frac{\gamma}{2m}\sin(\omega_r t)\right)\right), \quad (3)$$

and the force, ensuring the desired amplitude is reached takes the form

$$F_1 = F_{st-up} = F_0\left(1 - \frac{1}{1 + e^{\frac{\gamma}{2m}t_1}}\right) \approx \frac{F_0}{2}\left(1 + \frac{\pi}{4Q}\right) + \mathrm{O}\left[Q^{-2}\right], . \quad (4)$$

where the latter expression is valid in the high Q limit. The derivations of the solution (3) and expression for F_1 are outlined in Ref. 17.

Once the apex is reached the forcing can be turned to F_0 to hold the position x_0 at rest, as is illustrated in Figure 6. Alternatively, in scanning mode, a unipolar square wave can be applied to maintain the amplitude of the oscillating response. A plot of the drive force and response are illustrated in Figure 7 for a $Q = 10$ system and is constructed in the following way:

I) The step-up is expressed by equation 3 displaced by time t_0 so that $t \to (t - t_0)$ and the drive force is F_{st-up} given by equation 4. The step-up duration lasts t_1. or half a period of the damped system. In the high Q limit (introducing an error on the order of 0.2% of displacement at the peak for $Q = 10$) equation 3 becomes

$$x(t) = \frac{F_1}{k}\left(1 - e^{-\frac{\gamma(t-t_0)}{2m}}\cos(\omega_r(t - t_0))\right), \quad (5)$$

II) The response is set to ring for $N = 6$ full periods or $T_N = 6T_r = \frac{6}{f_r}$, after which a final pulse pulls all the energy out of the mode so that the resonator comes to rest at the origin. In a dissipationless system the forcing and response is symmetric. Including dissipation results in a second pulse which is smaller than the first as some of the energy is dissipated and does not need to be actively pulled out of the mode. One finds that the step-down force is

$$F_1 = F_{st-dn} = F_0 - F_{st-up} = \left(\frac{F_0}{1 + e^{\frac{\gamma}{2m}t_1}}\right) \approx \frac{F_0}{2}\left(1 - \frac{\pi}{4Q}\right) + \mathrm{O}\left[Q^{-2}\right], \quad (6)$$

and the amplitude response takes the form

$$x(t) = \frac{F_0}{k} - \frac{F_1}{k}\left(1 - e^{-\frac{\gamma t}{2m}}\left(\cos(\omega_r t) + \frac{\gamma}{2m}\sin(\omega_r t)\right)\right),$$
$$x(t) = \frac{F_{st-dn}}{k} + \frac{F_{st-up}}{k}e^{-\frac{\gamma t}{2m}}\cos(\omega_r t), \quad (7)$$

with the time shifted to $t_{dn} = t - t_0 - t_1 - t_N$. The second expression holds for large Q.

III) The cyclic period, in the example given here lasting 6 periods, is determined by solving equation 1 with $F_{dr} = 0$ N and F_1 switching on and off to form a uni-polar square wave with frequency $f_r = \frac{1}{T_r}$ and amplitude F_{SqW}. As two time-sections are implemented two sets of boundary conditions are needed: Initially, $F_1 = 0$ $x_a(t_1) = x_0$, and $x_a'(t_1) = 0$, corresponding to a release from rest at position x_0. A half-period later, $\frac{1}{2f_r}$, the force is switched to F_{SqW}.

The boundary conditions ensure a smooth continuity: $x_b\left(t_1 + \frac{T_r}{2}\right) = x_a\left(t_1 + \frac{T_r}{2}\right) = -x_0 e^{-\frac{\gamma\pi}{2m\omega_r}}$. and $x_b'\left(t_1 + \frac{T_r}{2}\right) = 0$. Finally, the force, F_{SqW}, needed to reach the target amplitude x_0 is determined by the condition that the apex is reached after a further half period, such that $x_b(t_1 + T_r) = x_0$. The sequence repeats N times until the energy is pulled from the mode as described previously. A closed form is given as:

$$x_a(t_a) = e^{-\frac{\gamma t_a}{2m}}\cos(\omega_r t_a)\left[0 < t_a < \frac{T_r}{2}\right]$$
$$x_b(t_b) = -e^{-\frac{\gamma t_b}{2m}}\cos(\omega_r t_b) + x_0\left[0 < t_b < \frac{T_r}{2}\right] \quad (8)$$

With $t_a = \mathrm{mod}(t - t_0 - t_1, T_r)$ and $t_b = \mathrm{mod}\left(t - t_0 - t_1 - \frac{T_r}{2}, T_r\right)$, and $t \in \left[t_0 + \frac{1}{2}T_r, t_0 + \left(N + \frac{1}{2}\right)T_r\right]$. Finally, the force required to remain "topped off" with a square wave drive is

$$F_{SqW} = F_0\left(1 - \frac{1 + e^{-\frac{\gamma\pi}{2m\omega_r}}}{1 + e^{\frac{\gamma\pi}{2m\omega_r}}}\right) \approx F_0\frac{\pi}{2Q}\left(1 - \frac{\pi}{4Q}\right) + \mathrm{O}\left[Q^{-3}\right]. \quad (9)$$

Figure 7 is generated by combining the results for the drive from equations 4 and 6 to generate the forcing for the step-up and down respectively, and equation 9 to maintain the resonant response. The amplitude response of the drive is plotted using equations 5, 7, and 8. The forcing starts at $t_0 = 1$ and the time is normalized to the period of the resonator. The solid black trace indicates the level of the step up and step-down forces for a dissipation free system, where for such a case no square-wave drive would be needed. As the forcing is only in one direction the response is no longer symmetric in amplitude with the negative deflection only reaching an amplitude of $-x_0 e^{-\frac{\gamma\pi}{2m\omega_r}}$. A numeric solution of the differential equation 1 is indistinguishable from the analytical solution.

Figure 8 illustrates how the different forcing amplitudes, scaled to the static force F_0, are affected by the quality factor. As would be expected the square wave forces, fall off for high Q. For high Q the step-up/ring-up forces converge as would be expected for a reversible dissipation free system. The step-down amplitude vanishes for low Q, as for such systems all energy is dissipated passively and there is no longer the need to actively apply a breaking force.

These algorithms depend on knowledge of the resonant frequency and quality factor of the scanner, but this is unlikely to be a limiting factor in performance. Silicon-based resonators have stable resonant frequencies with temperature variation (~31 ppm/°C) [21]. Additionally, on-chip thermometers allow for adjusting timings to shifts of the resonant frequency due to temperature changes. Humidity and pressure can also affect the resonant frequency, but the scanner can periodically measure its resonant frequency and quality factor to adjust for these changes. Additionally, even a high error of 0.5% would only cause a ringing of 0.5% of the step size using the galvo

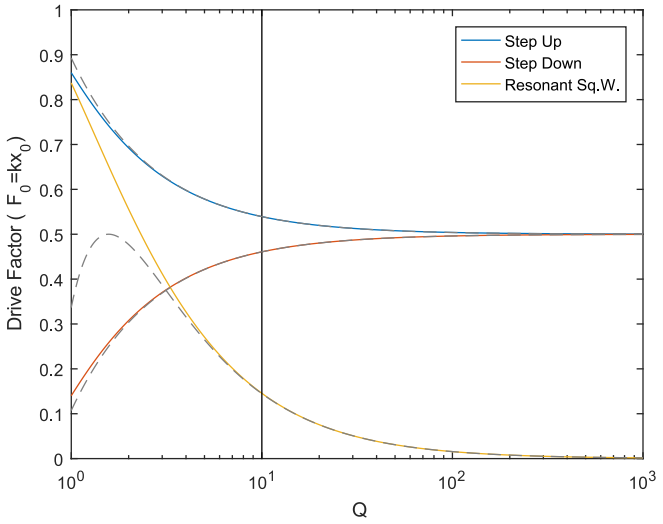

Fig. 8. Normalized drive forces as a function of the Quality factor. In each case the response amplitude is normalized to $x_0 = \frac{F_0}{k}$ and the solid line shows the exact solution while the dashed line shows the approximate solution. The yellow trace illustrates the drive force needed to maintain the amplitude of the resonant system for a unipolar square wave. As would be expected this falls off with increasing Q as the need to "top off" vanishes. Equation 9 gives the functional forms. The step up (blue line) and step-down (yellow line) drive forces converge at 0.5. The step-down force vanishes for low Q as all the energy in the mode is removed by dissipation and no breaking force is needed. The solid vertical black line corresponds to Q = 10, for which system the full responses are illustrated in figures 6 and 7.

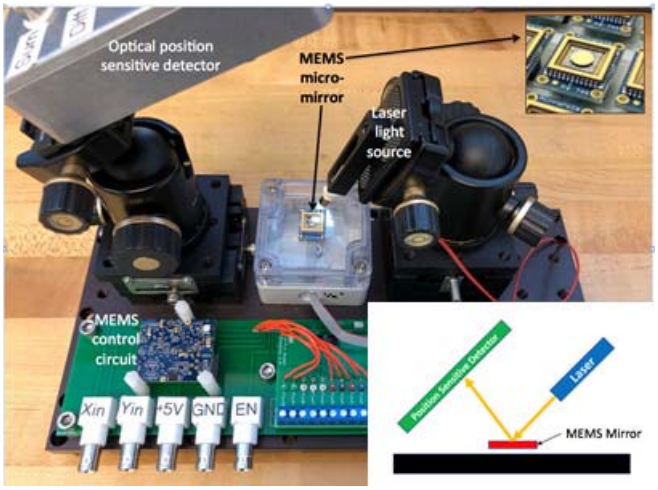

Fig. 9. Shown is our experimental apparatus. The Mirrorcle MEMS micro-mirror is mounted on the central section, illuminated with a laser and the position sensitive detector is used to detect the mirror's angular position. The mirror is controlled by an electronic circuit shown in the lower left of the photo.

control algorithm [16]. A similar error in amplitude is expected when using the scanner control algorithm to start oscillations. It may appear as though the error can be much larger when using the scanner algorithm to stop or reduce oscillations because the error on the period of every cycle would contribute to the error of the emptying pulse. This is only true for infinite or extremely high Q systems where no continuous driving is required. In most finite Q systems which require a continuous drive to "top off" the mode, the oscillation frequency is determined by the drive frequency and the error is not cumulative.

Instead of using square shaped pulses to fill/empty the mode, pulses made from parts of sine waves can be used, and instead of using a square wave to "top off" the mode, a sine wave can be used. In most systems, it will be simpler to use square pulse and square waves. However, to be complete, the derivation done here is repeated for sine shaped pulses and sine waves in supplemental information (S1).

IV. Experimental Results

To demonstrate these effects on a MEMS device, we have used a commercial micro-mirror system, the Mirrorcle Technologies product [22]. The device and system are shown in Figure 9. The device we used has a 5mm diameter mirror, a resonant frequency of 325 Hz and a packaged Q of 25. It is a Mirrorcle model A8L2.2 mirror, gimbal-less two axis bonded design with a gold-coated mirror and a tip/tilt range of $+/-5$ degrees about two axes.

Figure 9 also shows our experimental setup. The mirror is solidly mounted in the center of the system and a laser and position sensitive detector (PSD) are used to measure the mirror angles of rotation. For these experiments, we only use one axis of rotation. The mirror is controlled by an electronic drive circuit that determines the mirror angle. The drive circuit is supplied with the device by the manufacturer. A $+/-10$ V input creates a $+/-5$ degree rotation. The actual MEMS device itself is operated with ~180 V of drive. The electronic circuit has a look-up table with the device calibration stored on it and this system both creates the high voltage needed and corrects for the quadratic voltage dependence normally seen for a MEMS device. The input voltage to the system ($+/-10$ V) produces a linear angular response ($+/-5$ degrees) and so the input can be thought of as a force directly applied to the mirror. The electronic circuit is thus designed and calibrated to act like a fixed angular spring constant. The circuit is well fast enough to respond to the dynamics being studied here. An analog multiplier circuit (AD633) was used to modulate the input signal along with a summing circuit (from Stanford Research Systems) to add the various pulses together, created by an SRS DG645 pulse generator. The output of the PSD is proportional to the Sine of the angle change of the mirror. The output of the PSD can be adjusted to give the angle more exact angle change of the mirror. However, here we consider the output of the PSD to be approximately proportional to the angle change of the mirror because the range of the mirror is $+/-5$ degrees of rotation which makes it appropriate to apply the small angle approximation that $\sin\theta \approx \theta$.

Figure 10 shows experimental results. In the top panel, we show the native response of the system to a single step input. The $Q \sim 25$ and the system rings for many tens of milliseconds. The middle panel shows the response to a two-step input, similar to the simulations shown in Figure 1 and the analytical solutions shown in Figure 6. In the two-step input the settling time has been reduced to ~1/2 a period or ~1.5 ms from the ~100 ms of ringing seen in the upper panel. The small drop at the end is likely due to a small amount

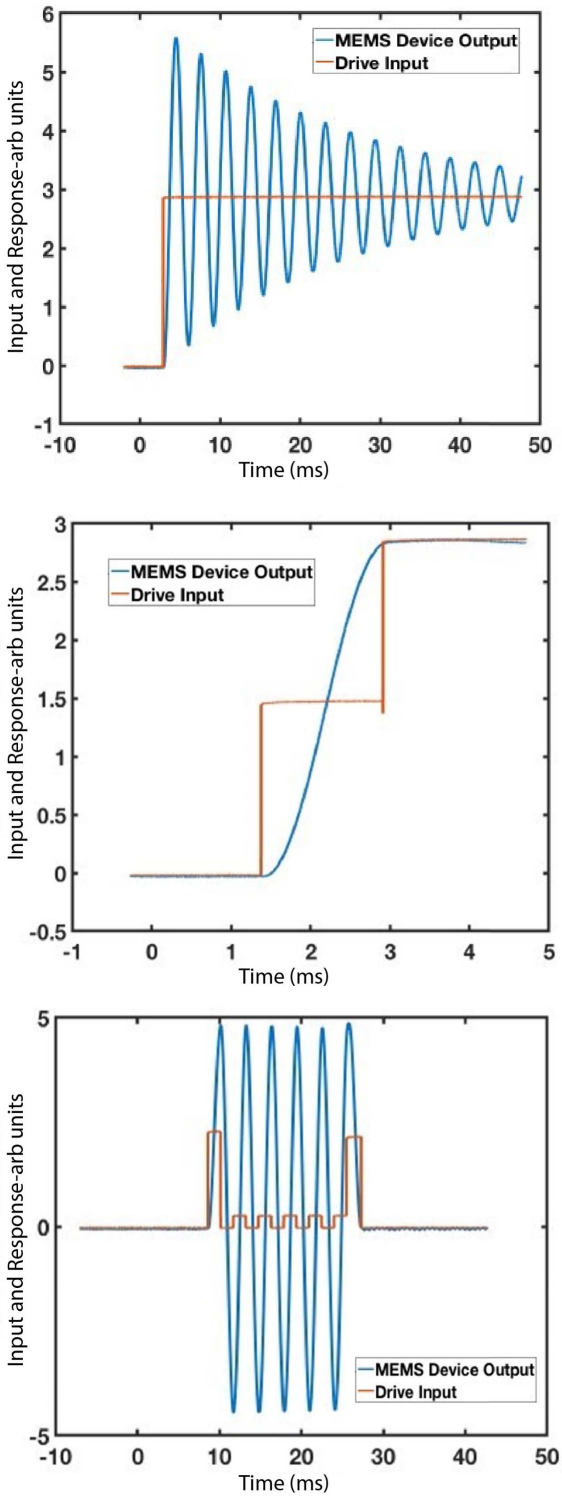

Fig. 10. Shown are results on the Mirrorcle MEMS micromirror using the algorithms described in the text. The red curve is the drive and the blue curve the device response. The upper panel shows the native response of the device. In response to a step input, it rings for ∼100ms. The middle panel shows the step response reduced to ∼1ms and the lower panel shows how one can use an advanced drive method to produce ideal scanner behavior. Note the differing time scales in all three plots. Red lines refer to input voltages which are proportional to forces because of the driving board.

of ringing due to error in the measurement of the resonant frequency. A more complete discussion of timing errors was provided by Imboden *et al.* [16].

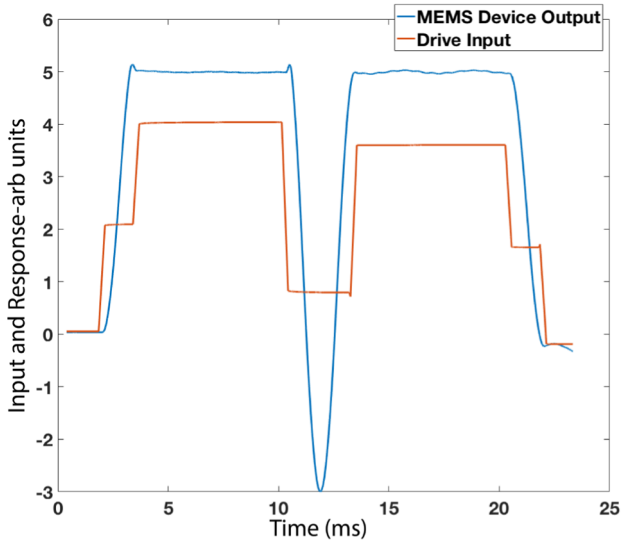

Fig. 11. Shown is a complex pattern of response of the MEMS device shown in Figure 9. This is a similar pattern to that shown in Figure 3. The red line refers to input voltages which are proportional to forces because of the driving board.

The lower panel shows the response to the drive algorithm for scanners, similar to the simulations in Figure 5 and the analytical solutions shown in Figure 7. The lower panel also shows a small amount of error in the amplitude of the oscillations. They appear to shrink through the first five cycles and then increase again on the last cycle. The shrinking through the first five cycles could be because the actual Q was slightly larger than the value use to calculate the amplitude of the square wave drive which would cause the oscillations to decrease until they reach the amplitude that corresponds to the driving oscillation. Alternatively, the shrinking could be due to the frequency being slightly off the resonance. In both cases, the system will stabilize in the transient or ringing time (∼100 ms). The system can be thought of ringing from the oscillation produced by the initial pulse to the oscillation corresponding to the square wave drive. The increase in the last pulse is likely due to the emptying pulse being too early.

Figure 10 shows how, by bringing both of the algorithms together on a real MEMS device, seamlessly move between galvo and scanner functioning to create complex patterns. The experimental results in Figure 11 can be compared with the simulation results in Figure 3. They agree, demonstrating the effectiveness of the algorithms discussed here. The difference in the shape of the inputs on Figure 3 and Figure 11 is due to Figure 11 being a finite Q system and Figure 3 being an infinite Q system.

V. Conclusion

In this paper we have shown how novel open loop control algorithms can make MEMS devices perform as essentially ideal galvos and scanners. In a real device, with a finite Q, changes to the input cause the system to ring and the response time is not ideal. For an optical system, the device is non-functional while ringing because it is not in a well-defined state. Using the algorithms shown here, one can make a high Q system respond in half a period.

Scanners can be driven using pulse to start the oscillation and a well timed second pulse to end the oscillations. For a finite Q device, an oscillating drive is added to compensate for the energy loss due to damping. Galvos can be driven using the two step drive described by Imboden *et al.* [16]. Combining these drives allows devices to move seamlessly between scanner and galvo functioning creating complex responses. This is demonstrated here with computer simulations, analytical models, and experimental results with a commercially available MEMS mirror.

This approach complements our previous work, where we have often presented unique device design and an optimized step-and-settle. These feedforward control algorithms enable ideal scanner and galvo motion, even with PWM control. Such an approach is appropriate for our MEMS micromirror with full hemispheric coverage [7] and for our five degrees-of-freedom scanner [6], as it supplements unique device design with practical control methods. We also build off other practical control discoveries, such as how to improve step-and-settle times using PWM [16] and how to perform analog control of MEMS devices [17], although the latter technique does not use the natural frequency of the device.

The algorithms we have presented here enable new design space for high-Q optical devices by overcoming ringing challenges without forcing design trade-offs in the foundational design.

ACKNOWLEDGMENT

The authors would like to thank Thorlabs for providing the Mirrocle Technologies mirror used in this study.

REFERENCES

[1] D. J. Bell, T. J. Lu, N. A. Fleck, and S. M. Spearing, "MEMS actuators and sensors: Observations on their performance and selection for purpose," *J. Micromech. Microeng.*, vol. 15, no. 7, pp. S153–S164, Jul. 2005.

[2] C. Liu, *Foundations of MEMS*, 2nd ed. Upper Saddle River, NJ, USA: Prentice-Hall, 2012.

[3] M. K. Mishra, V. Dubey, P. M. Mishra, and I. Khan, "MEMS technology: A review," *J. Eng. Res. Rep.*, vol. 4, no. 1, pp. 1–24, Feb. 2019.

[4] S.-C. Chen and M. L. Culpepper, "Design of a six-axis micro-scale nanopositioner—μHexFlex," *Precis. Eng.*, vol. 30, no. 3, pp. 314–324, Jul. 2006.

[5] M. Imboden *et al.*, "Atomic calligraphy: The direct writing of nanoscale structures using a microelectromechanical system," *Nano Lett.*, vol. 13, no. 7, pp. 3379–3384, Jul. 2013.

[6] L. K. Barrett *et al.*, "A large range of motion 3D MEMS scanner with five degrees of freedom," *J. Microelectromech. Syst.*, vol. 28, no. 1, pp. 170–179, 2019.

[7] C. Pollock, J. Javor, A. Stange, L. K. Barrett, and D. J. Bishop, "Extreme angle, tip-tilt MEMS micromirror enabling full hemispheric, quasi-static optical coverage," *Opt. Exp.*, vol. 27, no. 11, p. 15318, May 2019.

[8] S.-C. Chen, M. L. Culpepper, and S. C. Jordan, "Application of input shaping and hyperbit control to improve the dynamic performance of a six-axis MEMS nano-positioner," in *Proc. ASPE*, 2006.

[9] V. Milanovic and K. Castelino, "Sub-100 μs settling time and low voltage operation for gimbal-less two-axis scanners," in *Proc. IEEE/LEOS Opt. MEMS*, 2004.

[10] S. T. S. Holmstrom, U. Baran, and H. Urey, "MEMS laser scanners: A review," *J. Microelectromech. Syst.*, vol. 23, no. 2, pp. 259–275, Apr. 2014.

[11] J. B. Hopkins, R. M. Panas, Y. Song, and C. D. White, "A high-speed large-range tip-tilt-piston micromirror array," *J. Microelectromech. Syst.*, vol. 26, no. 1, pp. 196–205, Feb. 2017.

[12] D. N. Burghes and A. Graham, *Introduction to Control Theory, Including Optimal Control*. Bristol, U.K.: Horwood, 1980.

[13] F. L. Lewis, D. Vraibie, and V. L. Syrmos, *Optimal Control*, 3rd ed. Hoboken, NJ, USA: Wiley, 2012, pp. 1–18.

[14] H. W. Yoo *et al.*, "MEMS-based lidar for autonomous driving," *e & i Elektrotechnik und Informationstechnik*, vol. 135, no. 6, pp. 408–415, Oct. 2018.

[15] D. Wang, C. Watkins, and H. Xie, "MEMS mirrors for LiDAR: A review," *Micromachines*, vol. 11, no. 5, p. 456, Apr. 2020.

[16] M. Imboden *et al.*, "High-speed control of electromechanical transduction: Advanced drive techniques for optimized step- and-settle response of MEMS micromirrors," *IEEE Control Syst. Mag.*, vol. 36, no. 5, pp. 48–76, Oct. 2016.

[17] C. Pollock *et al.*, "Engineered PWM drives for achieving rapid step and settle times for MEMS actuation," *J. Microelectromech. Syst.*, vol. 27, no. 3, pp. 513–520, Jun. 2018.

[18] C. Pollock, L. K. Barrett, P. G. D. Corro, A. Stange, T. G. Bifano, and D. J. Bishop, "PWM as a low cost method for the analog control of MEMS devices," *J. Microelectromech. Syst.*, vol. 28, no. 2, pp. 245–253, 2019.

[19] M. Li, Q. Chen, Y. Liu, Y. Ding, and H. Xie, "Modelling and experimental verification of step response overshoot removal in electrothermally-actuated MEMS mirrors," *Micromachines*, vol. 8, no. 10, p. 289, Sep. 2017.

[20] B. Borovic, A. Q. Liu, D. Popa, H. Cai, and F. L. Lewis, "Open-loop versus closed-loop control of MEMS devices: Choices and issues," *J. Micromech. Microeng.*, vol. 15, no. 10, pp. 1917–1924, Oct. 2005.

[21] B. Jiang, S. Huang, J. Zhang, and Y. Su, "Analysis of frequency drift of silicon MEMS resonator with temperature," *Micromachines*, vol. 12, no. 1, p. 26, Dec. 2020, doi: 10.3390/mi12010026.

[22] (2013). *Mirrorcle Technologies MEMS Mirrors—Technical Overview*. [Online]. Available: https://www.mirrorcletech.com/wp/

Lawrence K. Barrett received the B.S. degree in applied physics and the M.S. degree in physics from Brigham Young University in 2014 and 2015, respectively, and the Ph.D. degree in materials science and engineering from Boston University in 2020. His research interests include MEMS design and control, nanomanufacturing, carbon nanotubes, graphene, and advanced chemical vapor deposition techniques.

Matthias Imboden received the Diploma degree in physics from Bern University in 2003 and the Ph.D. degree in physics in low-temperature nano-mechanics from Boston University in 2012. He held two postdoctoral positions, one in the Electrical and Computer Engineering Department at Boston University and the other as a Marie Skłodowska-Curie Fellow at the École Polytechnique Fédérale de Lausanne (EPFL). His current research interests include MEMS actuators and their control systems, bio-mechanics and soft actuators, as well as high-temperature micro-systems.

Joshua Javor received the B.S. degree in mechanical engineering from Ohio State University in 2016, where he studied the electromagnetic detection of solid cancerous tumors for his bachelor's thesis and the Ph.D. degree in MEMS/NEMS biomedical sensors from Boston University in 2021. His research interest includes the development of tools to study the interaction of electromagnetic, mechanical, and electrical interactions with engineered and native human cardiac tissue.

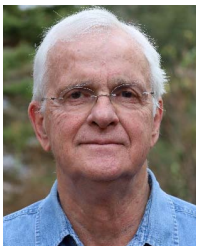

David K. Campbell received the B.A. degree in chemistry and physics from Harvard University in 1966 and the Ph.D. degree in theoretical physics and applied mathematics from Cambridge University in 1970. He is currently Professor of physics, electrical and computer engineering, and materials science and engineering. His current research interests include nonlinear and quantum effects in nanoscale materials such as graphene and engineered NEMS devices.

David J. Bishop (Member, IEEE) received the B.S. degree in physics from Syracuse University and the M.S. and Ph.D. degrees in physics from Cornell University. He is currently the Director of CELL-MET, an NSF ERC, and also the Head of the Division of Materials Science and Engineering, Boston University. He is also a Professor of physics, mechanical engineering, electrical and computer engineering, biomedical engineering, and materials science and engineering with BU. He was the Interim Associate Dean of Research and Graduate Programs with the College of Engineering, BU. Prior to joining BU, he was the Chief Technology Officer (CTO) and the Chief Operating Officer (COO) of LGS. Before joining LGS, he was the President of Government Research and Security Solutions for Bell Labs, Lucent Technologies. In previous positions with Lucent, he has served as the Nanotechnology Research VP for Bell Labs, Lucent Technologies; the President of the New Jersey Nanotechnology Consortium, and the Physical Sciences Research VP. He is a member of the National Academy of Inventors and the National Academy of Engineering. He is a fellow of Bell Labs, a fellow of the American Physical Society, and the winner of the APS's George E. Pake Prize for scientific leadership.